

Towards Reliable Die and Wire Bonding Processes in SpO₂ Sensor Manufacturing

Eero Mynttinen

School of Electrical Engineering

Thesis submitted for examination for the degree of Master of
Science in Technology.

Espoo, 24 November 2025

Thesis supervisor: Prof. Ivan Vujaklija

Thesis advisor: M.Eng. Teemu Äärynen

Author: Eero Mynttinen

Title: Towards Reliable Die and Wire Bonding Processes in SpO₂ Sensor Manufacturing

Date: 24 November 2025 Language: English Number of pages: 6+40

Department of Automation and Electrical Engineering

Professorship: Electronic and Digital Systems

Supervisor: Prof. Ivan Vujaklija

Advisor: M.Eng. Teemu Äärynen

Reliable die and gold wire bonding are essential for achieving consistent performance and high manufacturing yield in SpO₂ sensor sub-assemblies. However, limited prior understanding of bond formation mechanisms and parameter interactions in the existing production process created uncertainty around which factors most strongly influence bond integrity. In addition, prototype builds exhibited inconsistent wire bond quality, prompting a structured two-stage design of experiments (DOE) to identify the key parameters affecting wire bond strength and process capability. The results indicate that ultrasonic gain is the dominant factor influencing shear strength, with bonding force contributing to a lesser but still measurable extent. Bonding time affects bond quality only up to approximately 15 ms, after which its influence diminishes. Pull strength remained stable across parameter variations due to consistent neck-break failure modes. Several parameter combinations demonstrated low variation and high process capability, indicating feasible process windows for production use. Additional exploratory tests investigated free-air-ball formation, heat affected zone characteristics, and the influence of substrate temperature. Die bonding challenges were assessed in parallel, focusing on substrate pad height uniformity, epoxy coverage, and mechanical downholder configuration. Overall, the work provides a clearer understanding of the bonding mechanisms and the critical process parameters that influence the mechanical integrity of gold wire bonds, offering a solid basis for future validation and process optimization.

Keywords: design of experiments (DOE), die bonding, wire bonding, SpO₂

| | | |
|---|-----------------|-----------------|
| Tekijä: Eero Mynttinen | | |
| Työn nimi: Kohti luotettavia die- ja lankabondausprosesseja SpO ₂ -sensorien valmistuksessa | | |
| Päivämäärä: 24 November 2025 | Kieli: Englanti | Sivumäärä: 6+40 |
| Sähkötekniikan ja automaation laitos | | |
| Professuuri: Elektroniset ja digitaaliset järjestelmät | | |
| Työn valvoja: Prof. Ivan Vujaklija | | |
| Työn ohjaaja: M.Eng. Teemu Äärynen | | |
| <p>Luotettavat die- ja lankabondausprosessit ovat keskeisessä asemassa SpO₂-sensorin optisten alikokoonpanojen valmistuksessa. Prosessin toimintamekanismien sekä kriittisten prosessiparametrien ymmärrys oli kuitenkin puutteellista, minkä lisäksi protosarjat toivat esiin ongelmia molemmissa prosesseissa, mutta pääpainopisteeksi valittiin lankabondaus, jota tutkittiin kirjallisuuskatsauksen sekä kaksiosaisen koesuunnittelun (DOE) avulla. Mekaanista suorituskäkyä arvioitiin leikkaus- ja vetolujuuskokeilla.</p> <p>Leikkauslujuuteen vaikuttivat eniten ultraäänienergia ja bondausvoima, kun taas vetolujuus pysyi lähes muuttumattomana. Tämä selittyy todennäköisesti vetolujuustestin toistuvalla vikamoodilla, jossa lanka katkeaa systemaattisesti bondauspallon juuresta. Koesuunnittelun toinen osa osoitti parametriryhmien tuottavan matalat variaatiokertoimet sekä korkeat prosessin suorituskäkyindeksit, mutta bondauksen aika nousi bondausvoimaa merkittävämmäksi arvoksi. Voidaan olettaa, että 15 ms kohdalla saavutetaan lähes täysi bondaus. Lisäksi tehtiin eksploratiivista tutkimusta vapaan pallon (FAB) muodostumisesta, lämpövaikutusalueesta (HAZ) sekä substraatin lämpötilan vaikutuksesta. Die-bondauksen haasteita tarkasteltiin erikseen keskittyen substraatin pad-korkeuden vaihteluihin, epoksin levittymiseen ja mekaanisen downholder-komponentin konfiguraatioon.</p> <p>Kokonaisuutena työ selkeyttää AuAl-sidoksen muodostumismekanismia sekä tunnistaa kriittiset prosessiparametrit, jotka vaikuttavat kultalankabondausten mekaaniseen eheyteen. Tulokset tarjoavat vakaan perustan jatkovalidoinnille ja prosessin optimoinnille.</p> | | |
| Avainsanat: koesuunnittelu (DOE), die bondaus, lankabondaus, SpO ₂ | | |

Contents

| | |
|--|------------|
| Abstract | ii |
| Abstract (in Finnish) | iii |
| Contents | iv |
| Symbols and abbreviations | vi |
| 1 Introduction | 1 |
| 2 Background | 2 |
| 2.1 SpO ₂ Sensor | 2 |
| 2.2 Manufacturing Process | 2 |
| 2.3 Die Bonding | 3 |
| 2.4 Wire Bonding | 4 |
| 2.4.1 Theory of Wire Bonding | 6 |
| 2.5 Performance Assessment of Sensor Manufacturing | 7 |
| 3 Research material and methods | 8 |
| 3.1 Design of Experiments | 8 |
| 3.2 Die Bonding | 8 |
| 3.3 Wire Bonding Process in Detail | 11 |
| 3.4 Experimental Study on Wire Bonding Parameters | 12 |
| 3.4.1 Parameters and Setup | 14 |
| 3.5 Second Stage Experiments and Supporting Studies | 16 |
| 3.5.1 Comparative Study of Selected Parameter Levels | 16 |
| 3.5.2 Temperature and EFO Behavior Study | 17 |
| 3.6 Testing Methodology | 18 |
| 3.7 Statistical Evaluation and Process Capability Analysis | 20 |
| 4 Results | 21 |
| 4.1 Initial DOE | 21 |
| 4.2 Results of the Second Stage DOE | 23 |
| 4.2.1 Second-Stage DOE ANOVA | 24 |
| 4.2.2 Main and Interaction Effects | 24 |
| 4.2.3 Process Capability Calculations | 27 |
| 5 Discussion | 29 |
| 6 Conclusions | 33 |
| References | 34 |
| 7 Appendix | 36 |
| 7.1 Appendix 1 | 36 |

| | |
|--------------------------|----|
| 7.2 Appendix 2 | 38 |
|--------------------------|----|

Symbols and abbreviations

Symbols

| | |
|----------|--|
| σ | Standard deviation |
| C_{pl} | Process capability for lower specification limit |

Abbreviations

| | |
|------------------|------------------------------------|
| FAB | Free-air-ball |
| EFO | Electronic-flame-off |
| USG | Ultrasonic gain |
| HAZ | Heat affected zone |
| DOE | Design of experiments |
| SpO ₂ | Peripheral oxygen saturation |
| ANOVA | Analysis of variance |
| ICU | Intensive care unit |
| HbO ₂ | Oxyhemoglobin |
| Hb | Hemoglobin |
| TC | Thermocompression |
| gf | Grams of force |
| LSL | Lower specification limit |
| mils | Plural for a thousandth of an inch |

1 Introduction

Every day, millions of patients rely on pulse oximeters to monitor their blood oxygen levels—one of the key physiological indicators of health [1]. These sensors are utilized in patient monitoring throughout various clinical settings ranging from pre-hospital care to operating rooms (OR), intensive care units (ICU), and general wards [2].

The optical sub-assembly of a typical SpO₂ sensor consists of several key components: LEDs, a photodiode, the necessary interconnects, and a substrate. Although the device appears mechanically simple, its performance and reliability depend heavily on the quality of specific manufacturing process steps. Among these, die bonding (attaching semiconductor dies to the substrate) and wire bonding (forming electrical interconnections using fine wire) play a critical role in mechanical robustness, thermal stability, and electrical reliability.

For these reasons, this thesis focuses on understanding the die bonding and wire bonding processes that serve as the foundation of reliable SpO₂ sensor manufacturing. The primary goal is to identify the process parameters that influence bond integrity and yield in automatic gold wire bonding. The work consists of a literature review to establish the theoretical foundation and a design of experiments (DOE) study to quantify parameter effects and interactions. Die bonding challenges observed during prototype builds are also addressed to ensure sufficient die attach quality for downstream wire bonding.

The remainder of this thesis is organized as follows. Chapter 2 introduces the operating principle and components of the SpO₂ sensor, followed by the theory of die attach and wire bonding processes, and the approach to performance assessment of the manufacturing process. Chapter 3 details the research methods, including the bonding process setups, DOE methodology and setup, testing techniques, and statistical evaluation. Chapter 4 presents the experimental results, while Chapter 5 discusses the findings and introduces possible future improvements. Finally, Chapter 6 concludes the thesis by summarizing the main findings, drawing conclusions, and outlining potential directions for future work and process improvements.

2 Background

This chapter provides the theoretical and technical background necessary to understand the operation and manufacturing of the SpO₂ sensor studied in this work. The chapter first outlines the basic principle and clinical relevance of SpO₂ measurement, followed by an overview of the manufacturing processes used with a focus on the emitter and detector subassemblies, as these include the die and wire bonding steps examined in this thesis. Finally, the methods of assessing manufacturing performance and product reliability are discussed, laying the groundwork for the experimental work presented in the following chapter.

2.1 SpO₂ Sensor

This model of SpO₂ sensor uses red and infrared light to detect the oxygen bound to hemoglobin. The oxyhemoglobin (HbO₂) absorbs more infrared and less visible red, meanwhile the deoxyhemoglobin (Hb) absorbs more visible red and less infrared. These differences are then used to detect the amount of HbO₂ in the bloodstream [3]. The Beer-Lambert law is used as the foundation for how the light is attenuated when passing through a medium which contains matter capable of interacting with the light [3].

Given the basic operating principle of an SpO₂ sensor of this type, the list of components within the sensor are logical. The device has different LEDs for emitting the required light at different wavelengths, and a photodiode to measure and detect the differences in the amount of light absorbed in the medium.

The oxygen saturation is one of the most rudimentary, but also essential measurements to monitor and assess a patient's status. The clinical significance is relatively high, because oxygen plays such an important role in the human body and it is naturally tightly regulated. Any meaningful deviations from the normal are typically indicative of something that requires the attention of the medical professionals. Additionally, the SpO₂ value can be used to control the ventilator if the patient has been ventilated, for example in the ICU or the operating room [4]. Visible symptoms or signs of hypoxemia are often delayed or may be present only at severely low levels of oxygenation, thus promoting the importance of SpO₂ monitoring as a non-invasive, readily available way to give an early warning [5].

2.2 Manufacturing Process

The manufacturing process consists of several key steps, including die bonding, wire bonding, and encapsulation. Quality control inspections are typically carried out during and between the process steps to ensure bond integrity and overall quality. Depending on the production setup and supply chain, the encapsulated leadframes may either be singulated on-site or shipped as full units to downstream manufacturers for final sensor assembly.

2.3 Die Bonding

Common die attach methods include eutectic, solder, and adhesive bonding [6]. The latter can be performed using dispensed epoxies or pre-formed die attach films (DAF). In this work, the focus is on the epoxy-based adhesive bonding process utilized in this specific SpO₂ sensor manufacturing.

Bondline thickness (BLT) and fillet height are known to strongly influence die attach reliability [6]. Figure 1 illustrates the die attach configuration using an epoxy adhesive. The bondline thickness (BLT) and fillet height are both visible in the image. The bondline thickness represents the layer of epoxy separating the bottom of the die from the substrate surface. The fillet height, in contrast, refers to the extent of epoxy rising along the vertical sides of the die.

BLT is primarily affected by the amount of epoxy, bonding force, and the die cross section. Fillet height, on the other hand, is primarily affected by the amount of epoxy and capillary action, but the bondline thickness also plays a role. When the epoxy is displaced from beneath the die, it will be pushed to the sides, directly increasing the volume that forms the fillet.



Figure 1: Illustration of epoxy die bonding.

The primary effects on quality are not straightforward. Increasing the fillet height generally enhances mechanical support and die adhesion, allowing the die to withstand higher lateral forces before failure of the adhesion. A greater fillet also improves resistance to vertical pull forces, which is particularly relevant during wire bonding. However, in LED applications, an excessively high fillet formed from conductive epoxy may interfere with the intended current flow within the die, introducing a potential negative impact on the device's performance. In GaAs-based LEDs, the conductive epoxy may bridge the p- and n-layers along the die edge, effectively diverting current away from the active region and thereby reducing luminous efficiency and overall electrical performance [6].

Bondline thickness (BLT), on the other hand, plays a more critical role in determining the epoxy coverage across the die cross-section. An excessive BLT may predispose the die to tilting or misalignment, while the combination of bondline thickness and coverage directly influences the thermal conductivity of the interface, which has a

particular importance in LED applications due to higher thermal load [6].

2.4 Wire Bonding

Bonding equipment can be categorized by the degree of automation as manual, semi-automatic, or fully automatic. In manual systems, the operator performs all positioning and bonding steps using mechanical controls and visual alignment, which limits throughput and repeatability. Semi-automatic systems automate certain motions, such as bonding or wire feeding, while still requiring manual alignment. Fully automatic bonders, however, use computer-controlled vision systems and programmable motion to achieve high repeatability and throughput, making them the standard in large-scale manufacturing.

However, in wire bonding, the bonding method is typically tied to the degree of automation: ball bonders are rarely, if ever, fully manual [7].

Among the available wire bonding methods, thermosonic ball bonding is the most widely used in microelectronics and sensor manufacturing of today. The method, first introduced by Alexander Coucoulas in 1970 [8], combines ultrasonic energy, mechanical force and pressure, and elevated temperature to form a metallurgical connection between the bonding wire and the bonding pad. Typically the wire material chosen is a ductile metal such as gold or copper, chosen for its bondability and electrical conductivity. First, a free-air-ball (FAB) is created at the end of the bonding wire by using an electronic-flame-off (EFO) system on the bonder and bonded to the pad under tightly controlled parameters of force, ultrasonic power, and temperature. The second bond, known as the stitch bond, is formed on the other connection point to complete the interconnection and break off the wire and ready it for the next wire bond. This method enables a cost efficient process with excellent repeatability, making it highly suitable for automated production with high throughput [7]. Figure 2 represents an illustration that goes through the different steps of the thermosonic ball bonding.

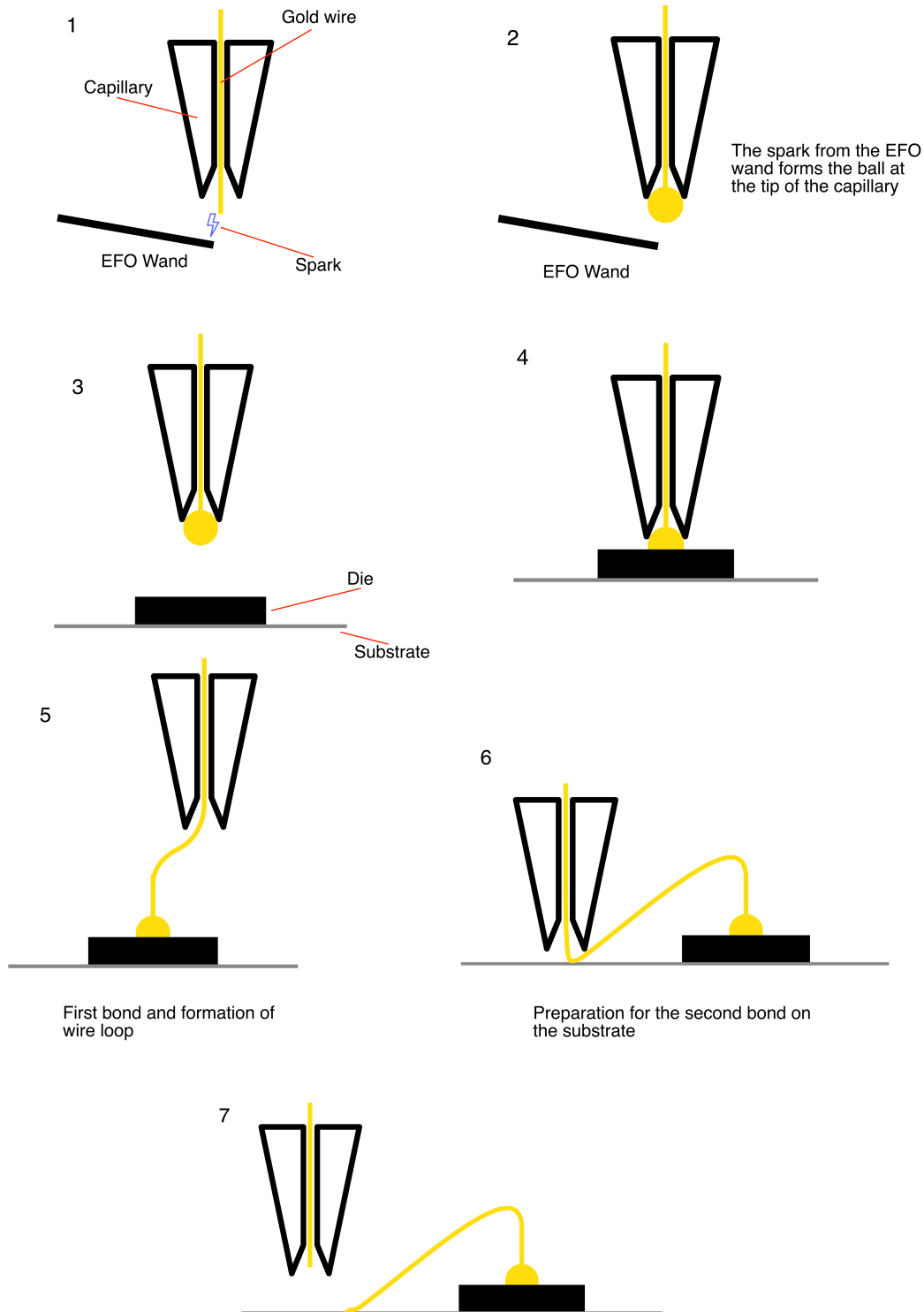


Figure 2: Simplified schematic of the thermosonic ball bonding process, illustrating the formation of the FAB, first bond, wire loop, and the second bond.

Step 1 and 2 show the creation of the free-air-ball with the spark from the EFO wand. In step 4 the gold ball is pressed against the bond pad of the die, where mechanical force and ultrasonic energy, together with heat, form the first metallurgical connection. In step 5, the capillary moves away from the second bond location to pull out excess wire to form the wanted wire loop tightness. In step 6 the capillary scrubs against the leadframe making the stitch bond and breaking off the wire. Step 7 just illustrates that the end of the gold wire is ready to receive another spark from the EFO to begin a new cycle.

2.4.1 Theory of Wire Bonding

While the previous section introduced the process flow of thermosonic ball bonding, this section examines the physical principles and material interactions that determine bond formation and reliability.

Thermosonic bonding combines the principles of ultrasonic and thermocompression (TC) bonding [7]. In thermocompression bonding, heat and pressure are used to form a solid-state bond between metals through diffusion and plastic deformation [9]. Ultrasonic bonding introduces high-frequency acoustic energy that reduces the required mechanical force to create plastic deformation necessary for wire bonding [10]. Because the ultrasonic energy reduces the need for high temperature and high mechanical force, the effects in combination enable strong and reliable bonds with reduced thermal and mechanical stress on the components.

While the bonding stress in TC bonding can be reduced by increasing the bonding duration, thermosonic bonding achieves comparable deformation much faster, enabling high-throughput manufacturing.

Based on the inherent nature of the thermosonic bonding process, the most relevant parameters for the practical experimentation were identified as ultrasonic gain, bonding force, bonding time, and temperature [11], [7].

The materials used for the bonding wire and the bonding pads, as well as the substrates beneath, affect the methodology and required parameters weights. In this study, the focus is explicitly on pure gold (Au) wire and aluminum (Al) bonding pad for the ball bond, and silver (Ag) coated copper (Cu) leadframe for the stitch bond.

Wire bonding with Au and Al can result in five different intermetallic compounds (IMCs): AuAl_2 , AuAl , Au_2Al , Au_4Al , and Au_5Al_2 , however, it has been debated that the Au_5Al_2 would actually be Au_3Al_8 [12], [13]. These intermetallic compounds (IMCs) start forming during the thermosonic bonding process due to the heat and ultrasonic energy, may continue to grow during later packaging or use if subjected to heat [7].

Among these, AuAl_2 (purple plague) is highly brittle and forms locally in overheated regions [14], while Au_3Al_8 (white plague) grows rapidly and may introduce Kirkendall voids due to unequal diffusion rates between Au and Al, resulting in porosity and

reduced bond reliability [7].

One key part of thermosonic ball bonding is the formation of the free air ball (FAB). As described earlier in Chapter 2.4, the EFO is used to recrystallize the gold at tip of the wire. The grain structure is very coarse in the ball section, and this heat bleeds into the wire above the ball itself creating the heat affected zone (HAZ). Here the grain structure of the wire is larger than in the rest of the wire due to the effect of heat from EFO application. The larger grain structure reduces the amount of grain boundaries, which reduces the mechanical strength of the wire [15]. The negative effects can possibly be mitigated by reducing the EFO current and time [15], [7].

2.5 Performance Assessment of Sensor Manufacturing

The performance of a sensor manufacturing process is typically evaluated through a combination of yield, consistency, product reliability, and throughput.

Yield represents the proportion of assemblies that meet the defined acceptance criteria and is often used as an indicator of the process stability. Throughput, in turn, reflects the production rate and efficiency of the process. It depends not only on the level of automation and process optimization, but also on the proper upkeep and maintenance of the equipment, since downtime directly lowers the production output capability.

Bond quality is commonly assessed using mechanical and visual inspection methods, such as destructive pull and shear tests, optical microscopy, or X-ray imaging, to detect defects like bond lift-off, cratering, or wire deformation. Statistical process control (SPC) methods are also applied to monitor and characterize the key process parameters to ensure repeatability and consistent quality across production lots.

Mechanical bond strength is typically verified through destructive testing methods such as pull and shear tests. JEDEC (Joint Electron Device Engineering Council) provides the standards for these testing methods and serves as the primary industry reference for microelectronic interconnect reliability assessment. These standards specify the testing configurations, loading rates, and failure mode classifications to ensure comparability between different processes and equipment.

3 Research material and methods

This chapter presents the experimental design approach to evaluation and characterizing the wire bonding parameters, and an overview of the machine setups for these specific die and wire bonding processes in SpO₂ sensor manufacturing. The focus is to understand the effect of critical process parameters on the bond integrity and overall yield. The chapter begins by outlining the aim of the design of experiments and the rationale behind using this approach. Following that, detailed descriptions of the manufacturing processes, selected parameters, and experimental procedures are provided. Finally, a brief overview of the data-analysis and utilized methodology is given.

3.1 Design of Experiments

The wire bonding process involves multiple interdependent parameters, such as bonding force, ultrasonic power, time, and temperature, all of which can influence bond quality and yield. Because these parameters often interact in complex, non-linear ways, varying one factor at a time would not provide a comprehensive understanding of their combined effects.

To systematically investigate and optimize these parameters, a design of experiments approach (DOE) was adopted. DOE enables efficient experimentation by evaluating the main effects and interactions of process parameters on bond integrity and yield.

Compared to a trial-and-error approach, DOE provides a data-driven and statistically sound method for process analysis [16]. When properly executed, it allows identification of the most influential parameters and interactions in an efficient, objective, and reproducible manner.

3.2 Die Bonding

Die bonding was the first process step, carried out using the BESI ESEC 2100Hsⁱ automatic die bonder. It is an automatic bonder that uses advanced machine vision systems for dynamic adjustment of the leadframes, to find the dies on the wafer, and for accurate and reliable pick-and-place operations. Automatic pressure control systems enable precise application of die attach epoxy to control the fillet height and bondline thickness.

After machine initialization, the recipe for the specific die and leadframe type was loaded. The machine setup is mechanically adjusted to match the chosen recipe, with installing the corresponding die ejector and bond head parts. The epoxy dispenser configuration remained consistent across all sensor sub-assembly variants.

Once the correct tools were installed, the machine preparation continues by loading the materials, the leadframes and the wafer containing the dies. Several machine areas required adjustments before manufacturing could begin. These include epoxy dispensing capillary XY-offset correction, Z-height measurement of the capillary tip,

and measurement of the leadframe die pad heights. During the second stage, the pick-and-place operation, additional adjustments are made for wafer rotation, die alignment, pick height, and bond height.

The die bonder was supplied with two interchangeable sets of process equipment, allowing the configuration to be adapted according to the die dimensions. The LEDs used in the assembly came in two sizes, 250 x 250 μm and 400 x 400 μm , both of which could be bonded using the same tooling. On the other hand, the photodiodes are considerably larger, measuring approximately 2 x 2 mm and 3 x 3 mm, and therefore required different tooling.

The main difference lay in the die ejector design, which penetrates the wafer foil to release the die. The four-needle ejector used for larger dies has its needles located close to the corners of the die. This configuration provides stability during ejection and prevents die tilting. In comparison, the smaller LED dies are handled using a single-needle ejector, which pushes the die from the center. Because the needle radius is relatively large compared to the footprint of these LED dies, the risk of tilting remained minimal even with a single needle.

Additionally, the suction cup on the bond head differed between the two equipment sets. The ideal suction cup size is slightly smaller than the die surface area to ensure reliable pickup without excessive adhesion. For the smaller LED dies, the originally installed rubber suction cup proved too tacky, occasionally causing the dies to stick to the tool after placement. A plastic suction cup was later introduced to mitigate this issue. However, due to project schedule constraints and equipment availability, the process parameters for the new cup could not be fully optimized within the time frame of this thesis.

Instead of focusing on suction tool optimization, the effort was directed toward improving the epoxy dispensing process and leadframe flatness control. The first prototype build resulted in a low yield of approximately 27 %, primarily due to poor epoxy dot quality or completely missing adhesive. Variations in pad height were found to have a significant impact on bonding yield. In particular, adjustments to the mechanical downholder system to maintain pad flatness were identified as the key improvement to enhance LED bonding yield.

After focusing on the adjustments of the mechanical downholder, the LED attach yield increased substantially during the subsequent prototype build—from 27 % to nearly 100 % in the context of dies placed in correct locations. Some variation in the die rotation still occurred, possibly due to the excessive blow-off pressure to separate the die from the bond head. Optimizing this part related to the bond head suction cup and related bond parameters remains outside the scope of the thesis.

In contrast to the LED bonding process, the photodiode attach still presented some challenges. The leadframe design includes four parallel rows of photodiode pads, and the existing downholder configuration did not make sufficient contact across all rows. This occasional variation in pad height height resulted in epoxy trace variations

and incomplete die adhesion. A new in-house downholder solution was designed to improve contact uniformity, but its implementation and verification remained outside the time frame of this thesis. The concept will be validated in future prototype builds.

After the downholder optimization for the LED assemblies and the resulting improvement in yield, the die bonding process achieved stable and repeatable performance. The produced assemblies met the quality and positional requirements needed for subsequent wire bonding experiments. The photodiode bonding performance was also acceptable for prototyping and experimental study purposes at this stage.

3.3 Wire Bonding Process in Detail

The wire bonding process constitutes the main focus of this thesis. The objective was to evaluate and improve the reliability and yield of gold wire bonds within the SpO₂ sensor sub-assemblies. The aim of the experimental work was to identify key process parameters that influence bond strength and consistency, and to establish a repeatable process window ensuring adequate mechanical integrity for production.

The investigation was guided by the provided minimum specifications for bond pull and shear strength, which were used as acceptance criteria. Due to sufficient initial performance, limited project time, and limited material availability, a full design of experiments was not conducted for the emitter assemblies with the LEDs. Instead, the focus was placed on understanding the bonding behavior and process stability of the photodiode interconnections (Figure 3), which exhibited greater variability in early trials.

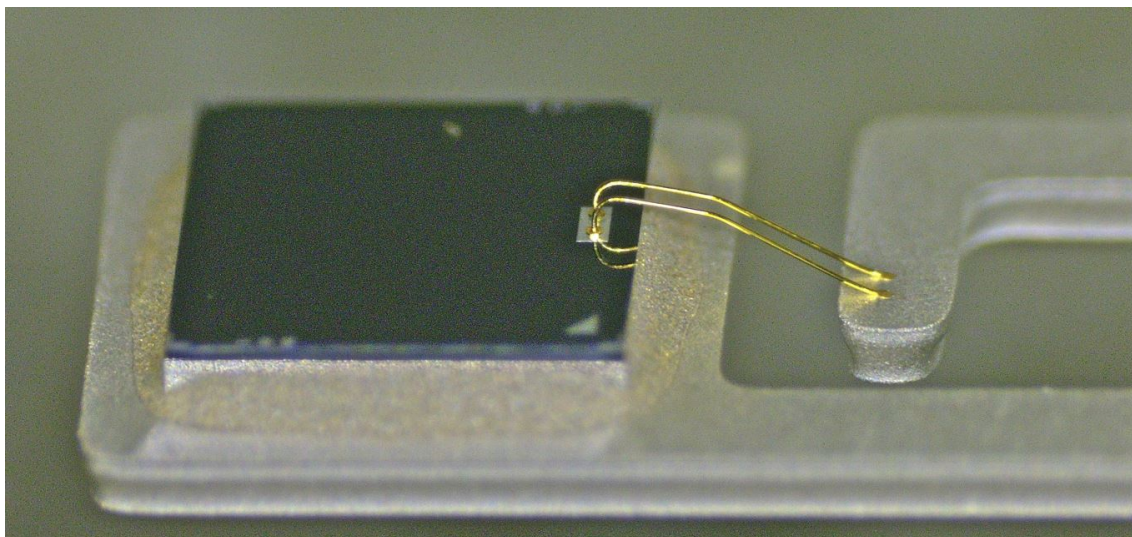


Figure 3: Image of the photodiode after die and wire bonding processes

All wire bonds were conducted using a Kulicke & Soffa RAPID automatic wire bonder. This machine uses advanced machine vision to locate the die and enables fast, reliable, and repeatable process with precise control over the process parameters. The bonder is a thermosonic ball bonder, and the bonding wire used across all sensor sub-assemblies is 1.25 mil (31.75 μm) pure gold (Au).

The machine includes several capabilities that were particularly relevant to this study. The heated material handling system, consisting of pre-bond, bond, and post-bond zones, allows controlled heating of the leadframe assembly. This promotes gold wire malleability and diffusion at the bond interface, which facilitates the plastic deformation of the wire and the formation of a stable metallurgical bond [7].

Different clamps and heat blocks are available for various leadframe designs, but all experiments for this thesis were conducted using a single leadframe configuration. This approach minimized material and bond program variation, ensuring consistent baseline conditions across all test builds. The materials chosen for this study were detectors with the photodiodes because of the inconsistent yield across two prototype builds. These dies are relatively large with aluminum (Al) bond pads.

The daily setup procedure consisted of selecting the correct bonding recipe, configuring the material handling system (MHS) with the corresponding heat block and clamp, and enabling the MHS heating. After the temperature has stabilized, the bonding wire is threaded, a bond-off is performed, and a new free-air ball (FAB) is formed. A few test samples are then bonded to verify proper wire feeding and bond placement. It is also advisable to perform destructive testing, particularly if the wire spool or capillary has been changed since the machine was last used.

Table 1 presents the capillary specifications. The selected capillaries are suitable for fine-pitch bonding conducted on a 32 μm wire.

Table 1: Capillary specifications used in wire bonding.

| Parameter | Specification |
|-------------------------|--|
| Capillary model | K&S H15 CD25 T55 OR5 F08 |
| Hole diameter (H15) | 1.5 mils ($\approx 38 \mu\text{m}$) |
| Chamfer diameter (CD25) | 2.5 mils ($\approx 64 \mu\text{m}$) |
| Tip diameter (T55) | 5.5 mils ($\approx 140 \mu\text{m}$) |
| Outer radius (OR5) | 0.5 mils ($\approx 13 \mu\text{m}$) |
| Face angle (F08) | 8° |

3.4 Experimental Study on Wire Bonding Parameters

The experimental study focused on the first (ball) bond formed between the gold wire and the aluminum pad, mainly due to the limited availability of testing equipment suitable for characterizing and evaluating the stitch bond. The test procedures for data acquisition for the DOE consisted of destructive pull and shear tests, as these directly reflect the mechanical strength of the wire bonds and are relatively easy and

fast to perform. The shear test explicitly targets the bonding interface, while the pull test stresses the whole system, indicating the weakest parts. Consequently, the process characterization and DOE results represent the behavior and strength of the first bond, which is also generally more critical to overall bond integrity.

A Design of Experiments (DOE) approach was used to systematically investigate the effect of selected bonding parameters on process performance and bond strength. Among various available experimental design strategies, the full factorial design was chosen for this study. In a full factorial design, all possible combinations of the selected factors and their levels are tested, enabling the simultaneous evaluation of both main effects and interaction effects [17]. This makes it a comprehensive method for understanding how process variables influence the outcome.

The full factorial design was particularly suitable for processes where multiple parameters may interact, as is the case in thermosonic wire bonding. Bonding force, ultrasonic power, and bonding time are interdependent, and changes in one may influence the optimal settings of the others [18]. By testing all combinations of parameter levels, it is possible to identify significant interactions and establish a process window that ensures stable and repeatable bonding performance.

The main limitation of the full factorial approach is the exponential increase in the number of required experiments as the number of factors and levels grows. For k factors and ℓ levels, a total of ℓ^k experimental runs are required. However, given the limited number of parameters investigated in this study, the full factorial method was considered feasible and the most informative option.

The results of the factorial experiments were analyzed using analysis of variance (ANOVA) and effects with $p < 0.05$ were considered statistically significant. ANOVA is a statistical method commonly applied to identify significant main effects and interactions in multi-factor experiments [19]. ANOVA quantifies how much each process parameter and their interactions contribute to the overall variation in the measured response. This makes it an effective tool for interpreting full factorial designs and verifying which parameters have statistically meaningful effects on bond integrity. The implementation details of the analysis are presented in Chapter 3.4.1.

3.4.1 Parameters and Setup

The baseline parameters were established based on previous experimentation and commissioning of the equipment.

Baseline parameters:

- Ultrasonic Gain (USG): 110 mA
- Bonding Force: 70 gf
- Bonding Time: 15 ms
- Temperature: 180 °C

Because the parameters and materials vary between applications, and most of the literature does not list the specific parameters used, the theoretical background for this process was relatively limited. Therefore, the aim of the full factorial study was to apply a wide range for each parameter to capture broad variations and identify general process trends. This approach allowed the main effects and interactions to be more easily distinguished and provided a foundation for further optimization if required.

A full factorial design with four factors at three levels would have required 81 samples. To conserve the limited available materials and reduce testing costs, temperature was excluded from the factorial study and kept constant at 200 °C. The resulting design included three factors (ultrasonic gain, bonding force, and bonding time) at three levels, requiring 27 samples in total. The chosen levels for each factor are listed in Table 2. The effect of temperature was evaluated separately in a later stage of the study.

Table 2: DOE factors and levels

| Factor | -1 | 0 | +1 |
|--------------------|-----------|----------|-----------|
| USG (mA) | 80 | 110 | 140 |
| Bonding Force (gf) | 30 | 60 | 90 |
| Bonding Time (ms) | 5 | 15 | 25 |

The sample and corresponding parameter level is visualized in the Table 3. The order is not randomized, and this decision was made deliberately. All of the samples will be made on the same leadframe, with same batch of wire, same capillary, and within a small timeframe. Therefore, the added complexity and difficulty of modifying the parameters in a completely randomized order was not deemed necessary, as the risk of environmental or production-related variation was considered minimal.

Table 3: DOE Matrix

| Sample | USG | Time | Force |
|--------|-----|------|-------|
| 1 | -1 | -1 | -1 |
| 2 | -1 | -1 | 0 |
| 3 | -1 | -1 | 1 |
| 4 | -1 | 0 | -1 |
| 5 | -1 | 0 | 0 |
| 6 | -1 | 0 | 1 |
| 7 | -1 | 1 | -1 |
| 8 | -1 | 1 | 0 |
| 9 | -1 | 1 | 1 |
| 10 | 0 | -1 | -1 |
| 11 | 0 | -1 | 0 |
| 12 | 0 | -1 | 1 |
| 13 | 0 | 0 | -1 |
| 14 | 0 | 0 | 0 |
| 15 | 0 | 0 | 1 |
| 16 | 0 | 1 | -1 |
| 17 | 0 | 1 | 0 |
| 18 | 0 | 1 | 1 |
| 19 | 1 | -1 | -1 |
| 20 | 1 | -1 | 0 |
| 21 | 1 | -1 | 1 |
| 22 | 1 | 0 | -1 |
| 23 | 1 | 0 | 0 |
| 24 | 1 | 0 | 1 |
| 25 | 1 | 1 | -1 |
| 26 | 1 | 1 | 0 |
| 27 | 1 | 1 | 1 |

The statistical analysis was conducted in MATLAB using a three-factor ANOVA to evaluate the effects of ultrasonic gain (USG), bonding time, and bonding force on the measured shear strength. The model included both main and two-way interaction effects, and Type III sum of squares was applied due to its independence from factor order, tolerance for unbalanced data, and ability to accommodate interactions. The analysis was performed using the `anovan` function in MATLAB. The corresponding syntax is provided in Appendix 7.1.

The results of this initial 3^3 factorial study served as the basis for refining the process parameters in a second-stage investigation. This follow-up study, described in Chapter 3.5.1, focused on a narrower parameter window to verify and quantify the most influential factors identified in the first DOE.

3.5 Second Stage Experiments and Supporting Studies

Following the initial full factorial DOE, additional studies were conducted to refine the bonding process and to extend the studies to include and analyze the pull strength as well. The aim of these studies was not only to include the pull test, but to also increase the statistical confidence by increasing the sample sizes and to assess the process stability through detailed statistical analysis, including process capability indices. Additionally, a further study was conducted to examine supporting factors that could influence bond integrity, such as bonding temperature and free-air-ball (FAB) formation behavior. This chapter presents the second-stage comparative DOE study in Chapter 3.5.1 and the supporting temperature and EFO investigations in Chapter 3.5.2. Furthermore, the destructive testing and process analysis methods are introduced in Chapters 3.6 and 3.7 respectively.

3.5.1 Comparative Study of Selected Parameter Levels

The second-stage DOE was designed to narrow the parameter ranges identified as most promising in the initial 3^3 factorial study and to improve statistical confidence through repetition. Additional testing was conducted using the parameter values listed in Table 4.

Table 4: DOE factors and levels.

| Factor | low | high |
|--------------------|------------|-------------|
| USG (mA) | 110 | 140 |
| Bonding Force (gf) | 60 | 90 |
| Bonding Time (ms) | 10 | 15 |

Table 5: Parameter groups

| Group | USG (mA) | Force (gf) | Time (ms) |
|--------------|-----------------|-------------------|------------------|
| 1 | 110 | 60 | 10 |
| 2 | 110 | 60 | 15 |
| 3 | 110 | 90 | 10 |
| 4 | 110 | 90 | 15 |
| 5 | 140 | 60 | 10 |
| 6 | 140 | 60 | 15 |
| 7 | 140 | 90 | 10 |
| 8 | 140 | 90 | 15 |

Full factorial DOE for ANOVA was conducted with 3 factors at 2 levels each for a total of 8 different sets of parameters. For redundancy and increased confidence, every set of parameters was used for 4 individual samples, so total sample size at this

stage was 32. However, the results and discussions refer to the 8 unique parameter sets presented in Table 5.

The aim of this part of the study was to add repetitions and gather data from smaller variations targeting especially the USG and bonding force values that provided the highest mechanical strength during the initial DOE stage.

These measurements were evaluated more in-depth. Using MATLAB, the coefficient of variation (CV), lower process capability index C_{pl} , mean values, and standard deviation were calculated and the results are provided in Chapter 4.2.3. MATLAB syntax is provided in Appendix 7.2.

3.5.2 Temperature and EFO Behavior Study

A small set of exploratory tests was conducted to examine whether bonding temperature, free-air-ball (FAB) formation, or electronic flame-off (EFO) behavior contributed to the neck-break failure mode (Figure 4) observed in pull testing. The study investigated:

- Bonding temperature between 200 °C and 250 °C
- FAB size (approximately 2.08x and 1.6x the wire diameter)
- EFO spark timing before and after the bonding cycle

These tests were performed outside the factorial DOE and were intended as supporting observations rather than part of the statistical analysis. Detailed mechanical testing showed no significant changes in pull or shear strength within the tested ranges. Because the effects were small and sample availability was limited, further examination was discontinued. The broader implications of these exploratory findings are discussed in Chapter 5.

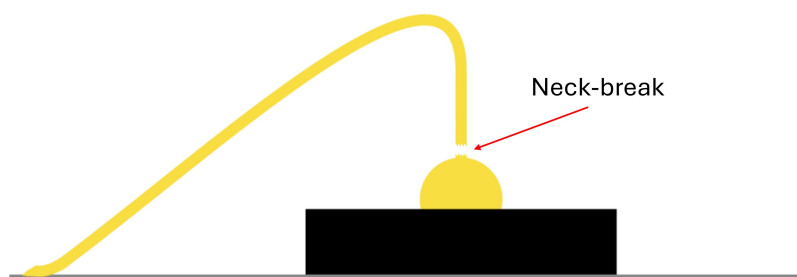


Figure 4: Illustration of the neck-break failure mode.

3.6 Testing Methodology

The destructive tests were conducted on a calibrated Xyztec Sigma tester. Pull test was conducted on top-of-the loop so the values here are directly comparable with pre-existing and subsequent process validation procedures.

The shear test values are represented in Table 6.

Table 6: Shear Test Parameters

| Parameter | Value | Unit |
|--------------------|--------------|-----------------|
| Test distance | 250 | μm |
| Test speed | 500 | $\mu\text{m/s}$ |
| Touchdown force | 5 | gf |
| Touchdown distance | 500 | μm |
| Touchdown speed | 100 | $\mu\text{m/s}$ |
| Shear height | 3 | μm |
| Shear speed | 200 | $\mu\text{m/s}$ |

The touchdown force was kept at a relatively low value, because the clamp of the tester does not make contact on the die pad directly. Therefore, it is possible it is raised slightly, pushed down during touchdown, and springs back up and reduces the shear height below the value set.

The Table 7 lists the pull test parameters.

Table 7: Pull Test Parameters

| Parameter | Value | Unit |
|------------------|--------------|-----------------|
| Test distance | 500 | μm |
| Test speed | 250 | $\mu\text{m/s}$ |

The Figure 5 portrays the test setup for the pull tests. The aim of the pull test was to replicate the Ball Pull Test as described by JEDEC in Standard No. B120.01 [20].

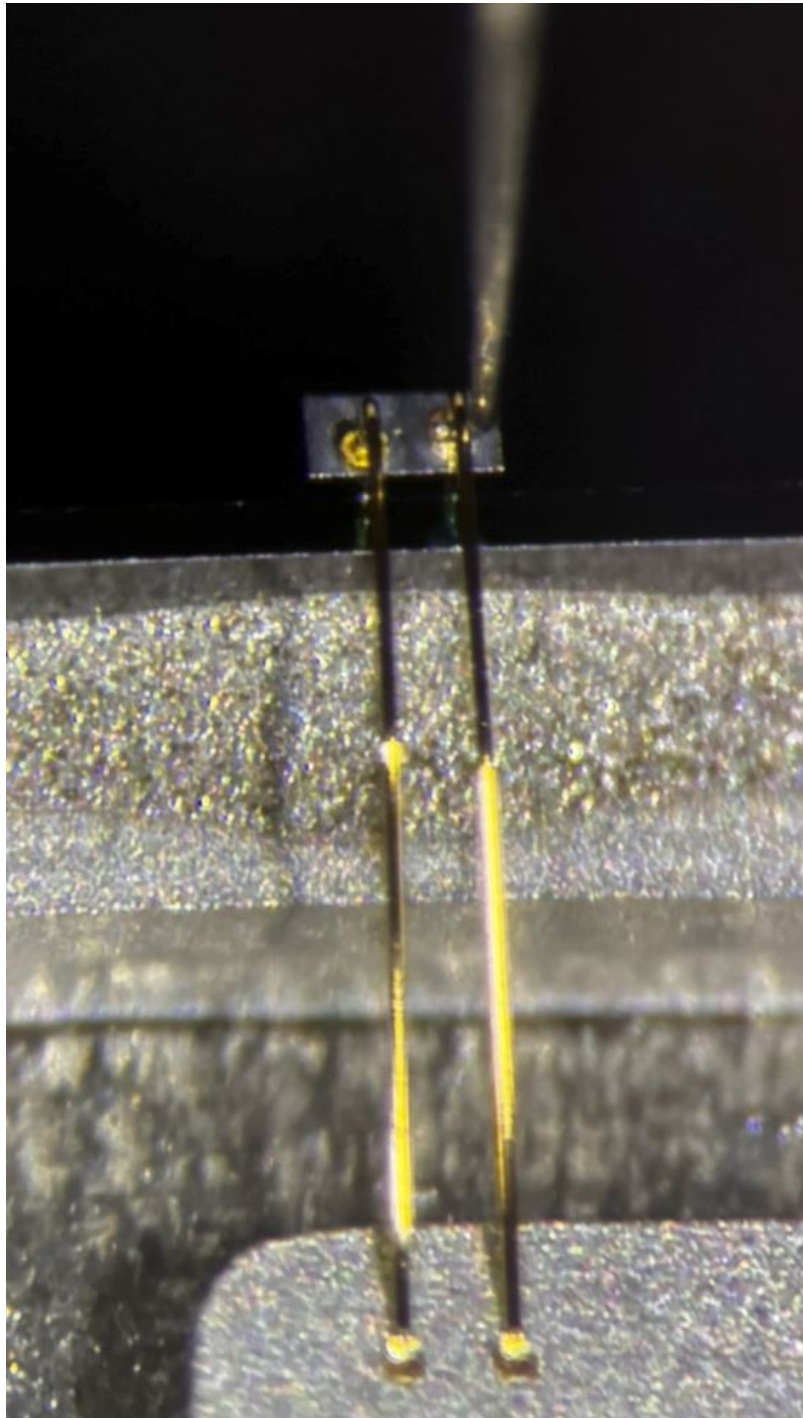


Figure 5: Image of the test hook placement used during pull tests. Hook is placed under the top-of-the loop for conducting the pull test.

3.7 Statistical Evaluation and Process Capability Analysis

The data collected from shear and pull testing were analyzed using statistical methods to quantify the influence of process parameters and assess process stability. Analysis of variance (ANOVA) was applied separately to the pull and shear strength data to identify statistically significant main and interaction effects among the tested parameters.

In addition, process capability indices were calculated to evaluate repeatability and compliance with the lower specification limit for bond strength during the second-stage DOE. The lower limit process capability index $C_{pl} = \frac{\bar{x} - LSL}{3\sigma}$ and coefficient of variation (CV) were selected as primary indicators of process robustness and reliability [21]. The values were calculated for both the shear and pull strength measurements acquired during the second-stage study presented in the Chapter 3.5.1 using the provided lower specification limits (LSL) of 10 gf for the pull and 25 gf for the shear.

These analyses provide a quantitative framework for comparing the performance of different bonding parameter combinations. The corresponding results are presented in Chapter 4.2.3 and discussed further in Chapter 5.

4 Results

This chapter presents the results of the experimental studies described in Chapter 3. The results are organized according to the two stages of experimentation: the initial shear strength based DOE and the subsequent extended DOE that included both shear and pull tests.

4.1 Initial DOE

The results of the ANOVA are summarized in Table 8, and the corresponding main and interaction effect plots are shown in Figures 6 and 7. The shear strength is displayed in grams of force on the Y-axis in both figures.

Table 8: Analysis of Variance (ANOVA) Summary

| Source | Sum Sq. | d.f. | Mean Sq. | F | Prob > F |
|------------|---------|------|----------|-------|-----------------------|
| USG | 3397.19 | 2 | 1698.59 | 58.91 | 1.63×10^{-5} |
| Time | 151.05 | 2 | 75.52 | 2.62 | 0.1333 |
| Force | 658.54 | 2 | 329.27 | 11.42 | 0.0045 |
| USG:Time | 25.02 | 4 | 6.25 | 0.22 | 0.9217 |
| USG:Force | 929.31 | 4 | 232.33 | 8.06 | 0.0066 |
| Time:Force | 320.30 | 4 | 80.07 | 2.78 | 0.1022 |
| Error | 230.66 | 8 | 28.83 | | |
| Total | 5712.05 | 26 | | | |

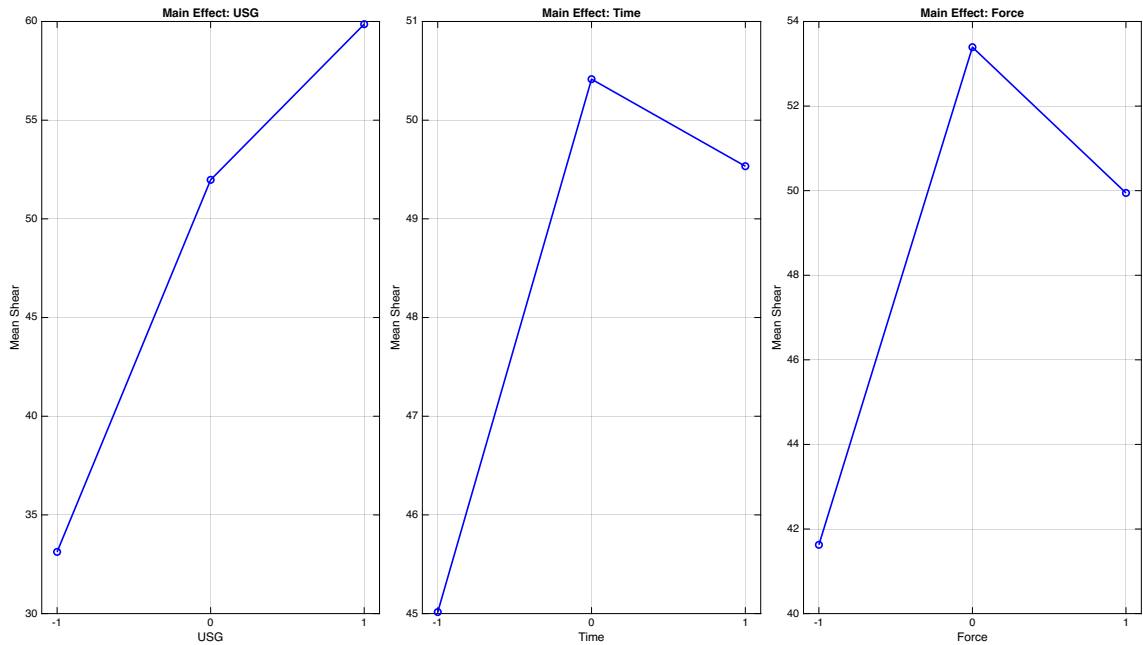


Figure 6: Main effects of individual parameters

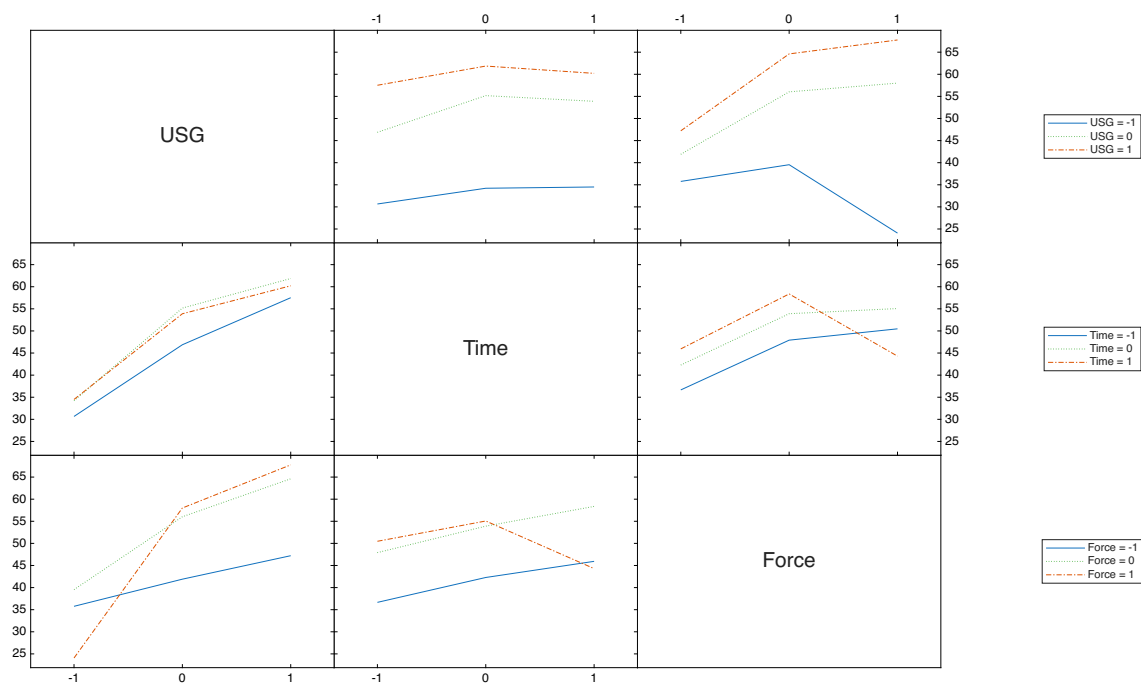


Figure 7: Interaction effects between parameters.

4.2 Results of the Second Stage DOE

This chapter goes through the results and findings related to the second DOE represented in Chapter 3.5.1.

Table 9: Four shear and pull strength measurements per group

| Group | Shear (gf) | Pull (gf) |
|--------------|-------------------|------------------|
| 1 | 49.19 | 13.00 |
| | 52.71 | 13.56 |
| | 55.14 | 13.54 |
| | 54.79 | 13.08 |
| 2 | 54.19 | 14.11 |
| | 64.47 | 11.85 |
| | 56.95 | 13.95 |
| | 57.52 | 13.29 |
| 3 | 52.76 | 13.51 |
| | 46.11 | 13.07 |
| | 48.95 | 13.48 |
| | 46.02 | 13.12 |
| 4 | 50.90 | 13.27 |
| | 61.63 | 13.42 |
| | 62.30 | 13.76 |
| | 54.95 | 13.53 |
| 5 | 63.76 | 13.44 |
| | 68.79 | 13.49 |
| | 65.75 | 13.36 |
| | 67.81 | 13.38 |
| 6 | 67.41 | 13.55 |
| | 71.11 | 13.63 |
| | 73.15 | 13.57 |
| | 70.63 | 13.12 |
| 7 | 70.17 | 13.47 |
| | 70.29 | 13.82 |
| | 70.33 | 13.82 |
| | 71.34 | 13.50 |
| 8 | 67.62 | 13.63 |
| | 69.12 | 13.32 |
| | 67.93 | 13.28 |
| | 67.33 | 13.28 |

4.2.1 Second-Stage DOE ANOVA

This section goes through the ANOVA results, which are listed in Table 10 for pull, and Table 11 for shear.

Table 10: Analysis of Variance for pull (Type III Sums of Squares)

| Source | Sum Sq. | d.f. | Mean Sq. | F | Prob > F |
|----------------|---------|------|----------|------|----------|
| USG | 0.14 | 1 | 0.14 | 0.82 | 0.37 |
| Time | 0.00 | 1 | 0.00 | 0.00 | 0.97 |
| Force | 0.06 | 1 | 0.06 | 0.34 | 0.57 |
| USG:Time | 0.09 | 1 | 0.09 | 0.54 | 0.47 |
| USG:Force | 0.00 | 1 | 0.00 | 0.01 | 0.93 |
| Time:Force | 0.01 | 1 | 0.01 | 0.05 | 0.83 |
| USG:Time:Force | 0.14 | 1 | 0.14 | 0.79 | 0.38 |
| Error | 4.11 | 24 | 0.17 | | |
| Total | 4.54 | 31 | | | |

Table 11: Analysis of Variance for shear (Type III Sums of Squares)

| Source | Sum Sq. | d.f. | Mean Sq. | F | Prob > F |
|----------------|---------|------|----------|--------|----------|
| USG | 1710.54 | 1 | 1710.54 | 174.83 | 1.64e-12 |
| Time | 125.22 | 1 | 125.22 | 12.80 | 0.0015 |
| Force | 7.62 | 1 | 7.62 | 0.78 | 0.3861 |
| USG:Time | 81.86 | 1 | 81.86 | 8.37 | 0.0080 |
| USG:Force | 22.88 | 1 | 22.88 | 2.34 | 0.1393 |
| Time:Force | 4.26 | 1 | 4.26 | 0.44 | 0.5155 |
| USG:Time:Force | 52.43 | 1 | 52.43 | 5.36 | 0.0295 |
| Error | 234.82 | 24 | 9.78 | | |
| Total | 2239.63 | 31 | | | |

4.2.2 Main and Interaction Effects

The pull test data did not show any statistically significant main or interaction effects according to the ANOVA results in Table 10; therefore, only the shear test results are visualized in Figures 8 and 9 respectively. The shear strength is displayed in grams of force on the Y-axis in both figures.

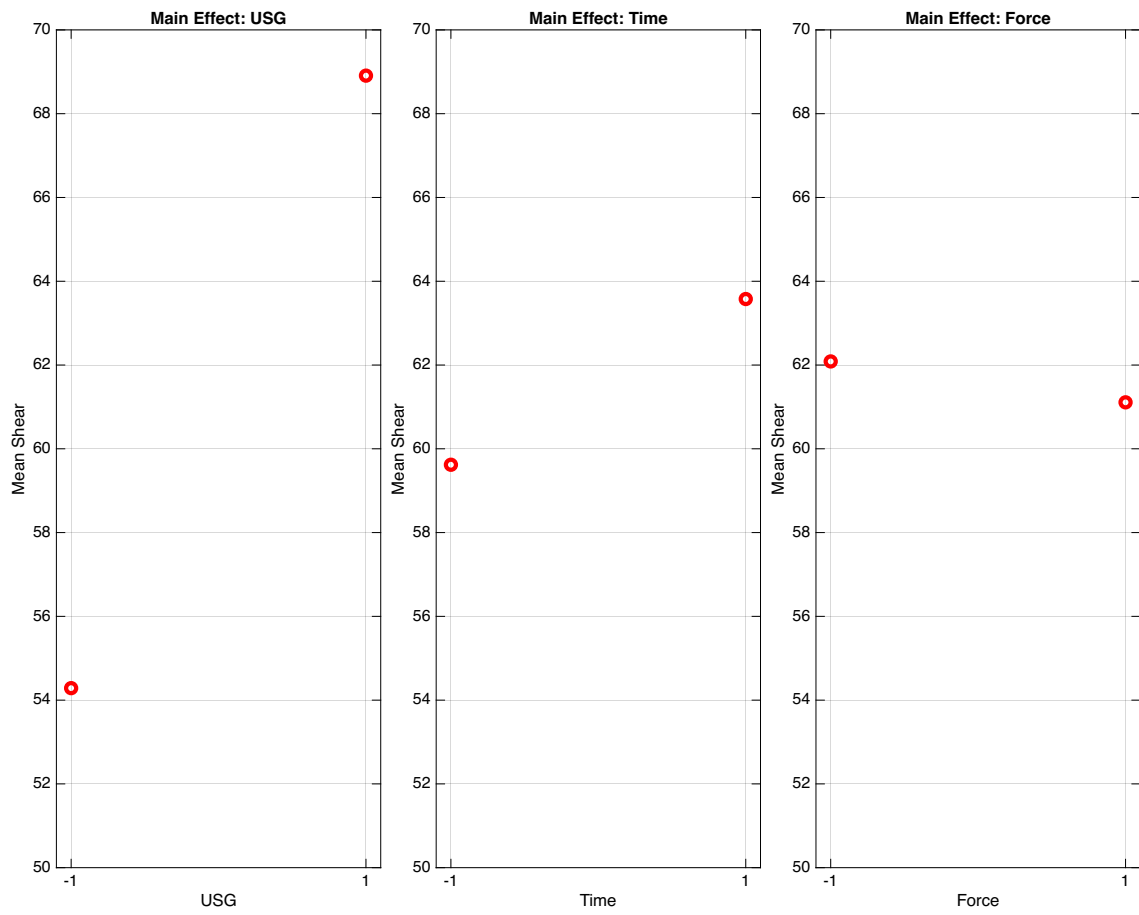


Figure 8: Main effects of individual parameters

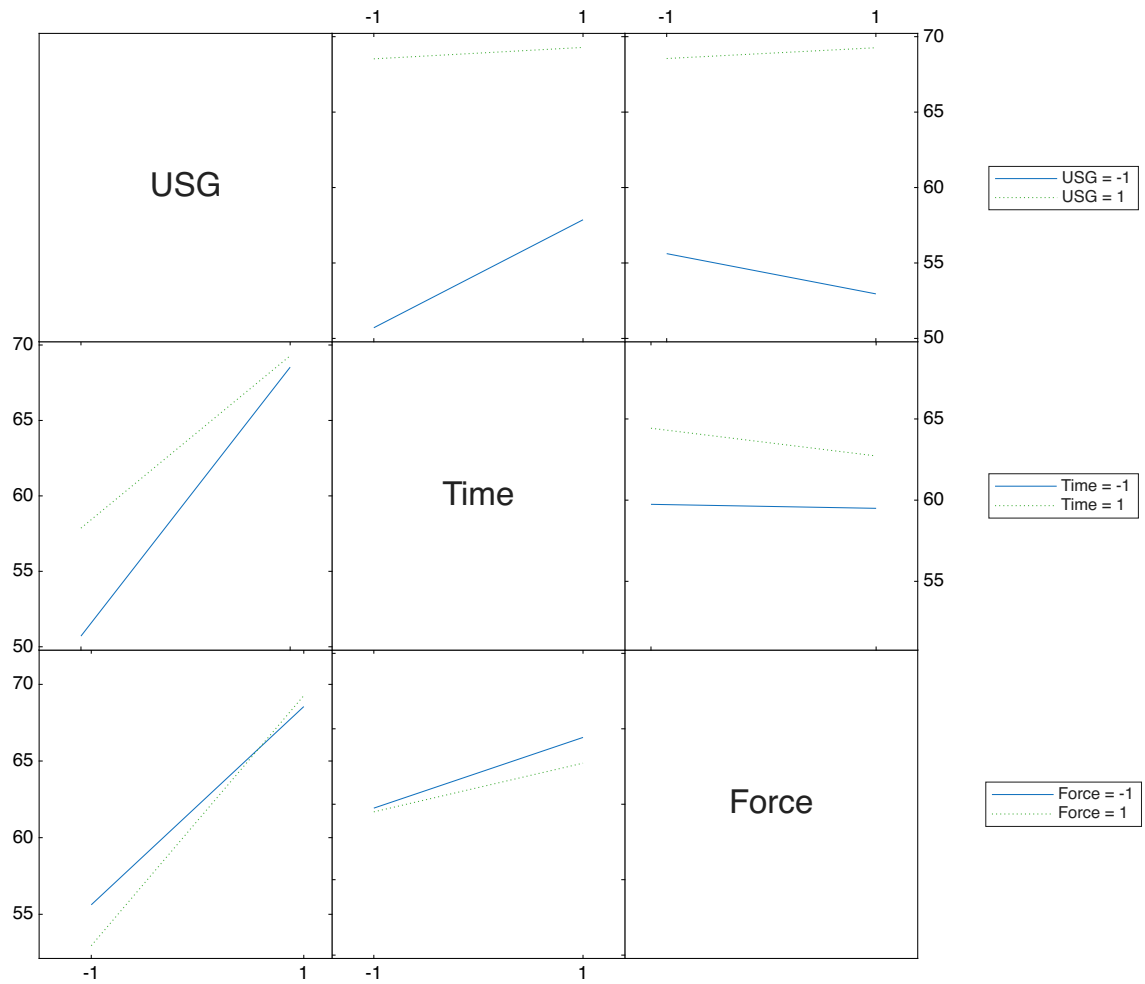


Figure 9: Interaction effects between parameters.

4.2.3 Process Capability Calculations

This section presents the results of the process capability evaluation, including mean and standard deviation, coefficient of variation (CV), and lower process capability index C_{pl} for both shear and pull strength measurements.

Table 12: Mean and standard deviation of shear and pull values for each parameter group.

| Group | Shear Mean (gf) | Shear SD (gf) | Pull Mean (gf) | Pull SD (gf) |
|-------|-----------------|---------------|----------------|--------------|
| 1 | 52.96 | 2.73 | 13.30 | 0.30 |
| 2 | 58.28 | 4.37 | 13.30 | 1.03 |
| 3 | 48.46 | 3.17 | 13.30 | 0.23 |
| 4 | 57.45 | 5.48 | 13.50 | 0.21 |
| 5 | 66.53 | 2.24 | 13.42 | 0.06 |
| 6 | 70.58 | 2.38 | 13.47 | 0.23 |
| 7 | 70.53 | 0.54 | 13.65 | 0.19 |
| 8 | 68.00 | 0.79 | 13.38 | 0.17 |

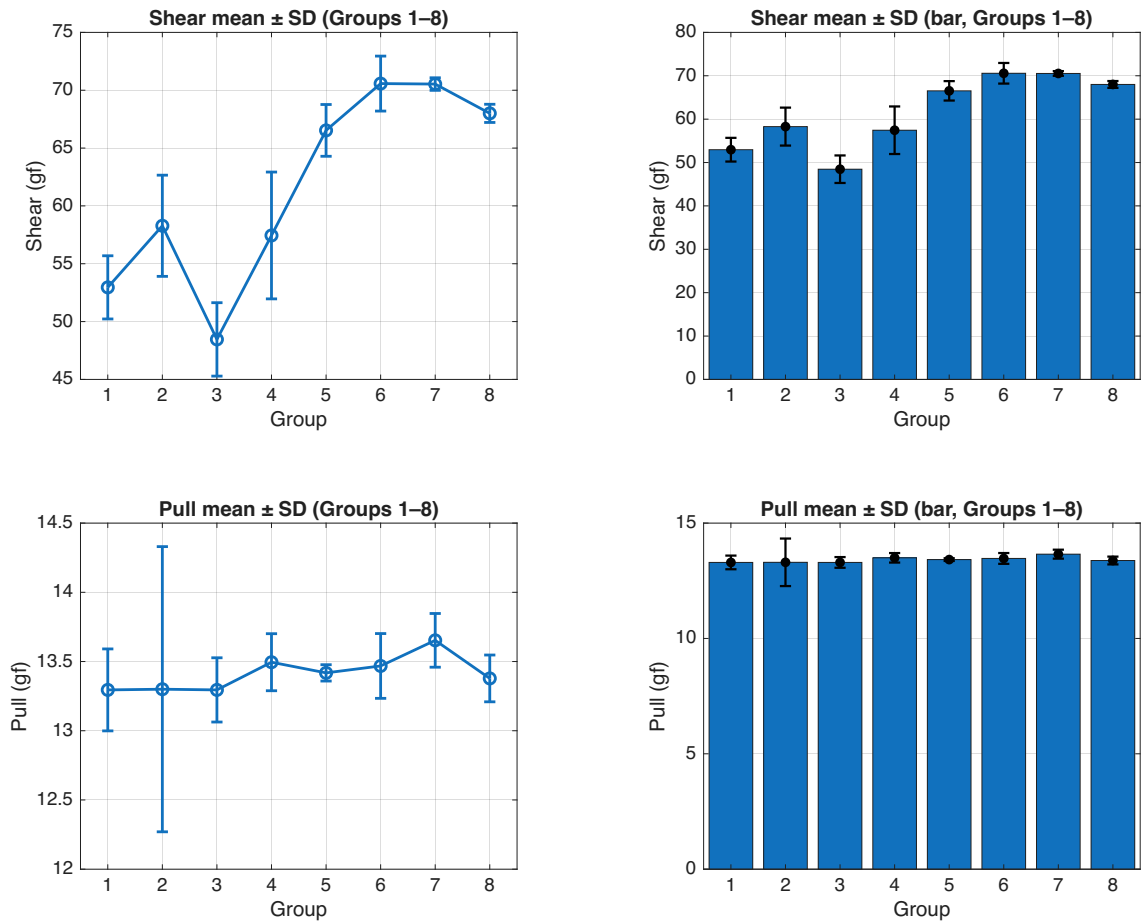


Figure 10: Mean and standard deviation visualized

Table 13: Coefficient of variation (CV) of shear and pull strengths for each parameter group.

| Group | Shear CV (%) | Pull CV (%) |
|--------------|---------------------|--------------------|
| 1 | 5.2 | 2.2 |
| 2 | 7.5 | 7.7 |
| 3 | 6.5 | 1.7 |
| 4 | 9.5 | 1.5 |
| 5 | 3.4 | 0.4 |
| 6 | 3.4 | 1.7 |
| 7 | 0.8 | 1.4 |
| 8 | 1.2 | 1.3 |

Table 14: Lower-sided process capability index (C_{pl}) for shear and pull strengths.

| Group | C_{pl} (Shear) | C_{pl} (Pull) |
|--------------|------------------------------------|-----------------------------------|
| 1 | 3.41 | 3.71 |
| 2 | 2.54 | 1.07 |
| 3 | 2.46 | 4.73 |
| 4 | 1.97 | 5.65 |
| 5 | 6.18 | 19.28 |
| 6 | 6.39 | 4.94 |
| 7 | 27.97 | 6.28 |
| 8 | 18.24 | 6.65 |

5 Discussion

This chapter discusses the results presented in Chapter 4 in greater depth. The focus is on interpreting the findings from the two stages of DOE, assessing the influence of key parameters on mechanical strength, and evaluating process robustness and reliability through statistical and data-driven analysis. The outcomes are further examined in the context of practical manufacturing implications, experimental limitations, and potential directions for future work.

The primary purpose of this thesis was to understand and characterize the critical process parameters in the gold wire bonding process related to the SpO₂ sensor sub-assembly manufacturing. Prototype builds exhibited inconsistent bonding performance, particularly in the photodiode assemblies, indicating that the existing bonding parameters were not fully optimized and that the interaction between process parameters, materials, and bond strength was not well understood. Wire bond reliability is critical for the overall performance and safety of the sensor, and therefore identifying a stable and repeatable process window for the wire bonding was essential for supporting future scale-up and validation of the manufacturing line. Although the primary focus of the thesis was on wire bonding, the upstream die bonding process was briefly discussed because it forms an essential part of the overall assembly flow and presented its own manufacturability challenges during the prototype builds.

For these reasons, a structured, statistical approach was required to achieve a systematic and data-driven understanding of the wire bonding parameters and their effects. The two-stage DOE in this thesis was designed to identify the key parameters influencing bond strength, quantify their interactions, and evaluate the process capability within practical manufacturing constraints. The discussion below connects these experimental findings to the underlying bonding mechanisms and to the broader manufacturing context, while also identifying areas where additional work is needed to fully qualify and validate the process.

Mashed ball geometry and bonded area were not characterized, so shear strengths are reported as absolute forces rather than area-normalized stresses. This means the values reflect relative comparative differences between parameter settings rather than absolute interface strength.

Starting with the first DOE, both the ANOVA and data plots presented in Chapter 4.1 support the idea of USG having the highest impact on shear strength. Additionally, bonding force contributes significantly to shear strength, though the data indicates a negative impact at the highest setting. The underlying reason was not experimentally verified, but it could possibly be explained by high bonding force restricting the ultrasonic motion through frictional damping and premature ball flattening, effectively reducing the lateral motion and negatively affecting the oxide disruption [7]. Bonding time had a measurable impact going from 5 ms to 15 ms but extending bonding time beyond that made practically no difference. The most probable explanation is that by ~ 15 ms the AuAl intermetallic layer has already formed across the full effective

contact area between the gold ball and the aluminum pad. Beyond this point, the interfacial metallization has essentially saturated, so extending the bonding time does not contribute additional bonding. The point of the first stage DOE was to observe general trends, and the limited sample size reduces statistical confidence, so the absolute values should be regarded as indicative rather than definitive.

The second-stage DOE further supports the findings of the first DOE regarding the shear test values. Especially USG, bonding time, and the combination of the two played a significant role in increasing the shear strength. The results suggest that a duration of approximately 15 ms represents the optimal saturation point for intermetallic formation, balancing bond strength with process efficiency. On the other hand, the tested parameters showed virtually no impact on pull strength as seen in Chapter 4.2. This outcome is consistent with the observed failure mode, which was predominantly a neck-break (visualized in Figure 4) rather than bond lift-off. Since the studied parameters mainly influence the bonding interface, their effects are not reflected in pull tests where failure occurs in a different region of the wire. Although ultrasonic gain (USG) can in principle influence neck area strength through localized thinning [7], the data from this study shows no measurable correlation with the pull values.

The process capability calculations presented in Chapter 4.2.3 focused on the coefficient of variation (CV) and the lower process capability index C_{pl} . The combination of relatively low CV values and consistently high C_{pl} values indicate that all eight parameter groups investigated in the second-stage DOE are statistically capable process settings with respect to the mechanical strength requirements. To assess the process capability, the mean values and standard deviations were calculated in Table 12 with the data visualized in Fig 10.

However, mechanical strength alone is insufficient to fully validate bond quality or long-term reliability. A comprehensive assessment must also consider mashed ball geometry, intermetallic compound (IMC) coverage and thickness, and die integrity—particularly the absence of cratering. As a result, the parameter set exhibiting the highest mean value and lowest standard deviation in mechanical tests does not necessarily represent the most reliable or robust process overall.

In contrast, the pull strength displayed consistent performance across all parameter groups, with the exception of one noticeably low value in the second group, which reduced the C_{pl} for that specific case. Given the small sample size, this deviation is likely attributable to a single outlier rather than a systematic process effect, and would be expected to average out with a larger dataset.

Because the bonding parameters in the DOE had no measurable influence on pull strength, additional exploratory tests were performed to determine whether FAB formation and the associated heat affected zone (HAZ) could explain or improve the observed neck-break behavior. Variations in FAB size (reduced incrementally from $2.08\times$ to $1.6\times$ wire diameter by lowering the EFO current), EFO spark timing, and material handling system (MHS) temperature (200–250 °C) produced no measurable

changes in pull strength within the limited sample size. A slight reduction in shear strength was observed with the smaller FAB, likely due to the reduced contact area, but this trend was not consistent enough to warrant further investigation. The EFO spark timing is typically utilized to prevent the FAB from cooling down between its formation and the bonding, and this method is often used in copper (Cu) wire bonding to improve the material bondability [7]. However, as the adjustments showed negligible influence on bondability, and gold is inherently softer material to bond, the experiments were discontinued to conserve materials and focus on the DOE studies.

Another factor influencing bond interface quality that was not evaluated in this study is the condition of the aluminum bond pads prior to wire bonding. Aluminum naturally forms a native oxide layer, and variations in oxide thickness can significantly affect bondability by increasing the energy required for oxide disruption during ultrasonic scrubbing. Techniques such as X-ray photoelectron spectroscopy (XPS) could be used in future work to characterize the thickness of the oxide layer on the pads before bonding. In addition, surface cleaning methods such as UV-ozone or plasma cleaning may help reduce oxide thickness and organic contamination, potentially lowering the USG and force requirements for reliable bonding [7]. This could in turn reduce the risk of cratering and further improve process robustness, especially for pads with variable surface conditions.

This study was also limited by the small sample size and the absence of a formal measurement system analysis on the Xyztec Sigma tester. Additionally, this study relies on the assumption that the wire bonder applies force, ultrasonic power, time, and temperature accurately as requested by the user. Independent verification of these parameters was not possible within the scope of the thesis. While these factors introduce uncertainty regarding measurement variation, the clear separation between parameter groups, the statistically significant effects observed in the ANOVA, and the low CV values across the DOE strongly indicate that the machine delivered consistent relative parameter levels. Substantial drift or inaccuracy would have resulted in overlapping distributions, reduced effect clarity, and degraded process capability, none of which were observed. For added certainty, future DOE studies could benefit from randomizing the production order to minimize any potential bias introduced by time-related or environmental factors.

Wire loop geometry was also not examined in this study. Parameters such as loop height, length, and overall shape can affect strain distribution and may influence long-term reliability, even if they are primarily constrained by packaging requirements.

While the primary focus of this thesis was the wire bonding process, the die bonding also plays a critical role in the manufacturing process of SpO₂ sensor sub-assemblies. The LED attach yield improved substantially after optimizing the mechanical downholder configuration, confirming that variations in the pad height are a critical factor in consistent epoxy application and subsequent die placement. However, some challenges remained with the larger photodiode dies: the redesigned, custom downholder intended to clamp all four rows of the leadframe was not completed in

time for evaluation. This solution could have mitigated pad height variations in a manner similar to the improvements observed for the LED assemblies. Although these limitations did not prevent execution of the wire bonding DOE, they highlight areas where further setup improvements could enhance die bonding consistency and, consequently, strengthen the robustness of the downstream wire bonding process.

Overall, the results of this work demonstrate that USG and bonding force are the dominant parameters affecting bond strength, and that a stable process window with high process capability can be achieved within the tested range. While the DOE-based optimization improved understanding of the key interactions, further metallurgical and surface-level analyses are needed to confirm long-term reliability. The findings provide a solid foundation for continued refinement of the bonding process and support the development of a more robust manufacturing flow for the SpO₂ sensor sub-assemblies.

6 Conclusions

This thesis characterized the key process parameters influencing the reliability and mechanical performance of gold wire bonding in the SpO₂ sensor sub-assembly manufacturing and established a statistically supported foundation for a stable bonding process. A two-stage DOE was used to quantify the effects of ultrasonic gain (USG), bonding force, and bonding time on bond strength and process capability.

The results identified USG and bonding force as the primary drivers of shear strength. However, the second-stage experiments demonstrated that bonding time also had a statistically significant impact on bond quality within the refined process window, particularly through its interaction with ultrasonic gain. Pull strength was largely unaffected by the bonding parameters due to the consistent neck-break failure mode, indicating that the weakest point was the heat affected zone (HAZ). The second-stage DOE confirmed these trends and demonstrated that all tested parameter combinations achieved high capability and low variability relative to the given mechanical strength requirements.

Although the DOE established a robust initial process window, mechanical strength alone cannot fully validate bond reliability. Future work should include assessment of mashed ball geometry, IMC coverage and thickness, and surface condition of the aluminum pads. Exploratory tests on FAB formation, EFO timing, and bonding temperature showed negligible impact, suggesting that further improvements may require metallurgical or surface-level analysis rather than additional parameter tuning.

While die bonding was not the primary focus, its influence as an upstream process was evident, and improved downholder contact had a direct impact on epoxy application and it could enhance overall assembly consistency.

In summary, this work provides a clear understanding of the dominant bonding parameters, a validated process window, and a framework for further optimization, supporting the development of a more reliable and scalable manufacturing process for the optical sub-assembly of the SpO₂ sensor.

References

- [1] A. Jubran, “Pulse oximetry,” *Critical Care*, vol. 19, no. 1, p. 272, 2015, ISSN: 1364-8535. DOI: [10.1186/s13054-015-0984-8](https://doi.org/10.1186/s13054-015-0984-8). [Online]. Available: <https://doi.org/10.1186/s13054-015-0984-8>.
- [2] U.S. Food and Drug Administration, “Review of pulse oximeters and factors that can impact their accuracy,” Center for Devices and Radiological Health, Silver Spring, MD, Executive Summary, Nov. 2022, Prepared for the Anesthesiology and Respiratory Therapy Devices Panel of the Medical Devices Advisory Committee meeting, November 1, 2022. Accessed: Oct. 29, 2025. [Online]. Available: <https://www.fda.gov/advisory-committees/advisory-committee-calendar/november-1-2022-anesthesiology-and-respiratory-therapy-devices-panel-medical-devices-advisory#event-materials>.
- [3] E. D. Chan, M. M. Chan, and M. M. Chan, “Pulse oximetry: Understanding its basic principles facilitates appreciation of its limitations,” *Respiratory Medicine*, vol. 107, no. 6, pp. 789–799, 2013, ISSN: 0954-6111. DOI: <https://doi.org/10.1016/j.rmed.2013.02.004>. [Online]. Available: <https://www.sciencedirect.com/science/article/pii/S095461111300053X>.
- [4] M. W. Semler et al., “Oxygen-saturation targets for critically ill adults receiving mechanical ventilation,” *New England Journal of Medicine*, vol. 387, no. 19, pp. 1759–1769, 2022. DOI: [10.1056/NEJMoa2208415](https://doi.org/10.1056/NEJMoa2208415). eprint: <https://www.nejm.org/doi/pdf/10.1056/NEJMoa2208415>. [Online]. Available: <https://www.nejm.org/doi/full/10.1056/NEJMoa2208415>.
- [5] B. B. Hafen and S. Sharma, “Oxygen saturation,” in *StatPearls [Internet]*, [Updated 2022 Nov 23], Treasure Island (FL): StatPearls Publishing, Jan. 2025. [Online]. Available: <https://www.ncbi.nlm.nih.gov/books/NBK525974/>.
- [6] D. Lu and C. Wong, *Materials for Advanced Packaging*, eng, 2nd ed. 2017. Cham: Springer International Publishing, 2017, ISBN: 3-319-45098-0.
- [7] G. Harman, *Wire Bonding in Microelectronics*, 3rd Edition. New York: McGraw-Hill Education, 2010, ISBN: 9780071476232.
- [8] A. Coucoulas, “Hot work thermosonic bonding, facilitating metal flow by restoration processes,” *Proceedings 20th Electronic Conference 1970*, Jan. 1970.
- [9] O. L. Anderson, H. Christensen, and P. Andreatch, “Technique for connecting electrical leads to semiconductors,” *Journal of Applied Physics*, vol. 28, no. 8, pp. 923–923, Aug. 1957, ISSN: 0021-8979. DOI: [10.1063/1.1722893](https://doi.org/10.1063/1.1722893). eprint: https://pubs.aip.org/aip/jap/article-pdf/28/8/923/18316983/923_1_online.pdf. [Online]. Available: <https://doi.org/10.1063/1.1722893>.
- [10] B. Langenecker, “Effects of ultrasound on deformation characteristics of metals,” *IEEE Transactions on Sonics and Ultrasonics*, vol. 13, no. 1, pp. 1–8, 1966. DOI: [10.1109/T-SU.1966.29367](https://doi.org/10.1109/T-SU.1966.29367).

- [11] H. Xu, C. Liu, V. Silberschmidt, Z. Chen, and J. Wei, “The role of bonding duration in wire bond formation: A study of footprints of thermosonic gold wire on aluminium pad,” *Microelectronics International*, vol. 27, pp. 11–16, Jan. 2010. DOI: [10.1108/13565361011009469](https://doi.org/10.1108/13565361011009469).
- [12] V. Koeninger, H. Uchida, and E. Fromm, “Degradation of gold-aluminium ball bonds by aging and contamination,” *IEEE Transactions on Components, Packaging, and Manufacturing Technology: Part A*, vol. 18, no. 4, pp. 835–841, 1995. DOI: [10.1109/95.477471](https://doi.org/10.1109/95.477471).
- [13] H. Xu et al., “A micromechanism study of thermosonic gold wire bonding on aluminum pad,” English, *Journal of Applied Physics*, vol. 108, no. 11, Dec. 2010, ISSN: 0021-8979. DOI: [10.1063/1.3514005](https://doi.org/10.1063/1.3514005).
- [14] C. W. Horsting, “Purple plague and gold purity,” in *10th Reliability Physics Symposium*, 1972, pp. 155–158. DOI: [10.1109/IRPS.1972.362544](https://doi.org/10.1109/IRPS.1972.362544).
- [15] S. Hu, R. Lim, and G. Sow, “Gold wire weakening in the thermosonic bonding of the first bond,” *IEEE Transactions on Components, Packaging, and Manufacturing Technology: Part A*, vol. 18, no. 1, pp. 230–234, 1995. DOI: [10.1109/95.370760](https://doi.org/10.1109/95.370760).
- [16] K. R. Bhote and A. K. Bhote, *World class quality : using design of experiments to make it happen*, eng, 2nd ed. New York: American Management Association, 2000, ISBN: 9780814426425.
- [17] D. C. Montgomery, *Design and Analysis of Experiments*, 9th ed. John Wiley & Sons, Inc., 2022, ISBN (EvalC): 9781119299455, ISBN: 9781119113478.
- [18] G. E. P. Box, J. S. Hunter, and W. G. Hunter, *Statistics for Experimenters: Design, Innovation, and Discovery*, 2nd ed. John Wiley & Sons, 2005, ISBN: 978-0-471-71813-0.
- [19] D. C. Montgomery, *Introduction to Statistical Quality Control*, 6th ed. Hoboken, NJ, USA: John Wiley & Sons, 2009, ISBN: 978-0-470-16992-6.
- [20] JEDEC Solid State Technology Association, *JESD22-B120.01: Wire Bond Pull Test Methods*, Revision of JESD22-B120, published December 2022, Arlington, VA, USA: JEDEC Solid State Technology Association, Dec. 2022. [Online]. Available: <https://www.jedec.org/standards-documents/docs/jesd22-b12001>.
- [21] DaimlerChrysler Corporation; Ford Motor Company; General Motors Corporation, *Statistical Process Control (SPC): Reference Manual*, 2nd ed. AIAG, 2005, Second Edition, issued July 2005.

7 Appendix

This section contains appendices.

7.1 Appendix 1

The following MATLAB script was used for statistical analysis and generation of the ANOVA table, main effects, and interaction plots presented in the results section.

Input was modified either by modifying the "data.xlsx" file, or supplying the "X" table more data manually.

The version uploaded here does ANOVA for pull test data, and plots for shear. These can be modified by changing between the value "Pull" and "Shear" in the corresponding function input.

```
clear; clc; close all;

data = readtable('data.xlsx'); %Filename here
%I had 5 columns in the file with following params:

USG = data.USG_mA;
Force = data.Force_gf;
Time = data.Time_ms;
Shear = data.Shear_gf;
Pull = data.Pull_gf;

X = table(USG, Time, Force, Shear, Pull);%Complex way of
renaming the data to X, at least gives you control
over column names and order. Easy to input more data

[p,tbl,stats] = anovan(Pull, {USG, Time, Force}, 'model',
'full', 'sstype', 3, 'varnames',{'USG','Time','Force
'}); %Default N-way analysis of variance, works
identical to minitab, for example

disp(p);

levels = [-1 0 1];
ME = struct();
```

```

for f = ["USG","Time","Force"]
    vals = zeros(size(levels));
    for i = 1:numel(levels)
        idx = X.(f) == levels(i);
        vals(i) = mean(X.Shear (idx));
    end
    ME.(f) = table(levels', vals', 'VariableNames', {char
        (f), 'MeanShear'});
end
figure('Name','Main Effects','Color','w');
tiledlayout(1,3,'Padding','compact','TileSpacing','
    compact');
%Plotting the main effects
for k = 1:3
    nexttile;
    f = ["USG","Time","Force"];
    T = ME.(f(k));
    plot(T.(char(f(k))), T.MeanShear, '-o', 'LineWidth'
        ,1.5, 'MarkerSize',6, 'Color','b');
    grid on;
    xlabel(sprintf('%s', f(k)), 'Color','k');
    ylabel('Mean Shear', 'Color','k');
    title(sprintf('Main Effect: %s', f(k)), 'Color','k');

    xlim([-1.1 1.1]);
    xticks([-1 1]);

    ax = gca;
    ax.XColor = 'k';
    ax.YColor = 'k';
end

LM_lin = fitlm(X, 'Shear ~ USG*Time + USG*Force + Time*
    Force'); % no quadratics
disp('--- Linear model with 2-way interactions ---');
disp(anova(LM_lin,'summary')); % ANOVA table, anovan
    already prints separate window, this goes to Command
    Window instead
disp(LM_lin);

% Interaction plots
figure('Name','Interaction Plots','Color','w');

```

```

interactionplot( X.Shear, {categorical(X.USG),
    categorical(X.Time), categorical(X.Force)}, 'varnames'
    , {'USG','Time','Force'});
ax = findall(gcf,'Type','axes');
for i = 1:numel(ax)
    ax(i).XColor = 'k';
    ax(i).YColor = 'k';
    ax(i).Title.Color = 'k';
    ax(i).XLabel.Color = 'k';
    ax(i).YLabel.Color = 'k';
end

```

7.2 Appendix 2

The following MATLAB script was used to calculate the means, standard deviations, coefficients of variation (CV) and lower-limit process capability index (C_{pl}) presented in Chapter 4.2.

It uses same foundation as Appendix 1, but expands on it with adding calculations and uploading those to the table. Additionally, the 8 unique parameter sets are divided here so the further calculations can be done based on the 4 individual samples that share the same parameter.

```

clear; clc; close all;

data = readtable('data.xlsx'); %Filename here
%I had 5 colums in the file with following params:

USG = data.USG_mA;
Time = data.Time_ms;
Force = data.Force_gf;
Shear = data.Shear_gf;
Pull = data.Pull_gf;

X = table(USG, Force, Time, Shear, Pull);

params = unique(X(:,1:3), 'rows', 'stable');

statsTbl = groupsummary(X, {'USG','Force','Time'}, {'mean',
    'std'}, {'Shear','Pull'});

disp(statsTbl)

```

```

statsTbl.Shear_CV = (statsTbl.std_Shear ./ statsTbl.
    mean_Shear) * 100;
statsTbl.Pull_CV  = (statsTbl.std_Pull   ./ statsTbl.
    mean_Pull)    * 100;

statsTbl.Shear_CV = round(statsTbl.Shear_CV, 1);
statsTbl.Pull_CV  = round(statsTbl.Pull_CV, 1);

disp(statsTbl(:, {'USG', 'Force', 'Time', 'mean_Shear', '
    std_Shear', 'Shear_CV', 'mean_Pull', 'std_Pull', 'Pull_CV'
    })))

LSL_shear = 25;    % gf
LSL_pull  = 10;    % gf

statsTbl.Cpl_shear = (statsTbl.mean_Shear - LSL_shear) ./
    (3 * statsTbl.std_Shear);
statsTbl.Cpl_pull  = (statsTbl.mean_Pull   - LSL_pull)   ./
    (3 * statsTbl.std_Pull);

statsTbl.mean_Shear = round(statsTbl.mean_Shear, 3);
statsTbl.std_Shear  = round(statsTbl.std_Shear, 3);
statsTbl.Shear_CV   = round(statsTbl.Shear_CV, 1);
statsTbl.Cpl_shear  = round(statsTbl.Cpl_shear, 2);

statsTbl.mean_Pull  = round(statsTbl.mean_Pull, 3);
statsTbl.std_Pull   = round(statsTbl.std_Pull, 3);
statsTbl.Pull_CV    = round(statsTbl.Pull_CV, 1);
statsTbl.Cpl_pull   = round(statsTbl.Cpl_pull, 2);

disp(statsTbl(:, { 'USG', 'Force', 'Time', 'mean_Shear', '
    std_Shear', 'Shear_CV', 'Cpl_shear', 'mean_Pull', '
    std_Pull', 'Pull_CV', 'Cpl_pull' })))

```